Exact Solution for Thermoelastic Deformations of Functionally Graded Thick Rectangular Plates

Senthil S. Vel*
University of Maine, Orono, Maine 04469-5711
and
R. C. Batra†
Virginia Polytechnic Institute and State University, Blacksburg, Virginia 24061

An exact solution is obtained for three-dimensional deformations of a simply supported functionally graded rectangular plate subjected to mechanical and thermal loads on its top and/or bottom surfaces. Suitable temperature and displacement functions that identically satisfy boundary conditions at the edges are used to reduce the partial differential equations governing the thermomechanical deformations to a set of coupled ordinary differential equations in the thickness coordinate, which are then solved by employing the power series method. The exact solution is applicable to both thick and thin plates. Results are presented for two-constituent metal–ceramic functionally graded rectangular plates that have a power law through-the-thickness variation of the volume fractions of the constituents. The effective material properties at a point are estimated by either the Mori–Tanaka or the self-consistent schemes. Exact displacements and stresses at several locations for mechanical and thermal loads are used to assess the accuracy of the classical plate theory, the first-order shear deformation theory, and a third-order shear deformation theory for functionally graded plates. Results are also computed for a functionally graded plate with material properties derived by the Mori–Tanaka method, the self-consistent scheme, and a combination of these two methods.

I. Introduction

ADVANCED composite materials offer numerous superior properties to metallic materials, such as high specific strength and high specific stiffness. This has resulted in the extensive use of laminated composite materials in aircraft, spacecraft, and space structures. For example, a layer of a ceramic material when bonded to the surface of a metallic structure acts as a thermal barrier in high-temperature applications. However, the sudden change in material properties across the interface between discrete materials can result in large interlaminar stresses leading to delamination. Furthermore, large plastic deformations at the interfaces may trigger the initiation and propagation of cracks in the material. One way to overcome these adverse effects is to use functionally graded materials in which material properties vary continuously. This is achieved either by gradually changing the volume fraction of the constituent materials, usually in the thickness direction only, or by changing the chemical structure of a thin polymer sheet to obtain a smooth variation of in-plane material properties and an optimum response to external thermomechanical loads. The former class of functionally graded structures can be manufactured by high-speed centrifugal casting[1,2] in which layers are formed in the radial direction due to different mass densities of the constituents, or by depositing layers of ceramic materials on a metallic substrate.[3,4] Lambros et al.[5] have developed an ultraviolet irradiation process to obtain variations in Young's modulus in the plane of a sheet. A directed oxidation technique has been employed by Breval et al.[6] and Manor et al.[7] to obtain a ceramic layer on the outside surface.

There are several three-dimensional solutions available for the thermoelastic analysis of inhomogeneous plates. Most of these studies have been conducted for laminated plates that have piecewise constant material properties in the thickness direction. Three-dimensional solutions for functionally graded plates are useful because they can be used as benchmarks to assess the accuracy of various two-dimensional plate theories. Rogers et al.[8] have employed the method of asymptotic expansion to analyze three-dimensional deformations of inhomogeneous plates. However, the boundary conditions on the edges of the plate in their theory are applied in an average sense like those in two-dimensional plate theories, and the plate is assumed to be only moderately thick. Tarn and Wang[9] have also presented an asymptotic solution that may be carried out to any order, but the manipulations become more and more involved as one considers higher-order terms, and numerical examples are given only for laminated plates consisting of homogeneous layers. Cheng and Batra[10] have also used the method of asymptotic expansion to study the three-dimensional thermoelastic deformations of a functionally graded elliptic plate.

Tanaka et al.[11,12] designed property profiles for functionally graded materials to reduce the thermal stresses. Reddy[13] has presented solutions for rectangular plates based on the third-order shear deformation plate theory. Reiter et al.,[14] Reiter et al.,[15] and Reiter and Dvorak[16] performed detailed finite element studies of discrete models containing simulated skeletal and particulate microstructures and compared results with those computed from homogenized models in which effective properties were derived by the Mori–Tanaka[17] and the self-consistent[18] methods. Cheng and Batra[19] have related the deflections of a simply supported functionally graded polygonal plate given by the first-order shear deformation theory (FSDT) and a third-order shear deformation theory (TSDT) to that of an equivalent homogeneous Kirchhoff plate. Lee and Yu[20] and Lee et al.[21] have expanded the mechanical displacements, the electric potential, and the material moduli as a power series in the thickness coordinate, derived plate equations of different orders for functionally graded piezoelectric materials, and analyzed their free vibrations. Batra[22] has studied finite plane strain deformations of a functionally graded incompressible hollow cylinder loaded by a uniform pressure on the inner surface.

The objective of this investigation is to present an exact solution to the three-dimensional thermoelastic deformations of a simply supported functionally graded rectangular thick plate. We assume that the plate is made of an isotropic material with material properties varying smoothly in the thickness direction only. By the use

*Assistant Professor, Department of Mechanical Engineering.
†Clifton C. Garvin Professor, Department of Engineering Science and Mechanics, M/C 0219.

of suitable temperature and displacement functions, the governing partial differential equations are reduced to a set of coupled ordinary differential equations in the thickness coordinate, which are solved by the power series method. We consider a two-phase graded material with a power law variation of the volume fractions of the constituents through the thickness. The effective material properties at a point are determined in terms of the local volume fractions and the material properties of the two phases either by the Mori–Tanaka[17] (also see Benveniste[23]) or by the self-consistent[18] scheme. Results are presented for an Al/SiC graded rectangular plate. Displacements and stresses at critical locations for mechanical and thermal loads are given for different length-to-thickness ratios, exponents in the power law through-the-thickness variation of the constituents, and different homogenization schemes. We compare the exact results with those obtained from the classical plate theory[24,25] (CPT), the FSDT,[26,27] and the TSDT.[27,28] The results from the three plate theories are quite different from the exact solution for thick functionally graded plates.

Results are also computed for a functionally graded plate for which the effective material properties in the ceramic rich and the metal rich regions are derived by the Mori–Tanaka[17] method, and the effective properties elsewhere are obtained by the self-consistent[18] scheme. A third-order transition function of Reiter and Dvorak[16] is used in the transition regions to have a smooth variation of material properties between the regions. For the thermal load, this combined method of homogenizing material properties gives plate deformations and transverse normal and transverse shear stresses that differ significantly from those computed with either the Mori–Tanaka or the self-consistent scheme alone. However, through-the-thickness variation of the longitudinal stress given by the three homogenization methods is essentially the same except at points near the top surface of the plate where the volume fraction of the ceramic is high. For the mechanical load, the homogenization technique influences strongly the transverse displacements but not the values of the stress components.

II.   Formulation of the Problem

We use rectangular Cartesian coordinates x_i, $i = 1, 2, 3$, to describe the infinitesimal static thermoelastic deformations of an N-layer laminated plate occupying the region $[0, L_1] \times [0, L_2] \times [-H/2, H/2]$ in the unstressed reference configuration. Each layer of the laminated plate is made of an isotropic material with material properties varying smoothly in the x_3 (thickness) direction only. The vertical positions of the bottom and the top surfaces and the $N - 1$ interfaces between the layers are denoted by $H^{(1)} = -H/2, H^{(2)}, \ldots, H^{(n)}, \ldots, H^{(N)}$ and $H^{(N+1)} = H/2$.

The equations of mechanical and thermal equilibrium in the absence of body forces and internal heat sources are (e.g., see Carlson[29])

$$\sigma_{ij,j} = 0 \tag{1a}$$

$$q_{j,j} = 0 \tag{1b}$$

where σ_{ij} and q_j are, respectively, the components of the Cauchy stress tensor and the heat flux vector, and where $i, j = 1, 2, 3$. A comma followed by index j denotes partial differentiation with respect to the position x_j of a material particle, and a repeated index implies summation over the range of the index.

The constitutive equations for a linear isotropic thermoelastic material are[29]

$$\sigma_{ij} = \lambda \varepsilon_{kk} \delta_{ij} + 2\mu \varepsilon_{ij} - \beta \delta_{ij} T \tag{2a}$$

$$q_j = -\kappa T_{,j} \tag{2b}$$

where λ and μ are the Lamé constants, β is the stress-temperature modulus, κ is the thermal conductivity, ε_{ij} are components of the infinitesimal strain tensor, T is the change in temperature of a material particle from that in the stress-free reference configuration, and δ_{ij} is the Kronecker delta. The material properties λ, μ, β, and κ are functions of x_3.

The infinitesimal strain tensor is related to the mechanical displacements u_i by

$$\varepsilon_{ij} = \tfrac{1}{2}(u_{i,j} + u_{j,i}) \tag{3}$$

The edges of the plate are assumed to be simply supported and maintained at the reference temperature. That is,

$$\sigma_{11} = 0 \tag{4a}$$

$$u_2 = u_3 = 0 \tag{4b}$$

$$T = 0 \tag{4c}$$

at $x_1 = 0$ and L_1 and

$$\sigma_{22} = 0 \tag{4d}$$

$$u_1 = u_3 = 0 \tag{4e}$$

$$T = 0 \tag{4f}$$

at $x_2 = 0$ and L_2.

The mechanical boundary conditions prescribed on the top and the bottom surfaces can be either a displacement component u_j or the corresponding traction component σ_{3j}. However, typically nonzero normal and zero tangential tractions are prescribed on these two surfaces. Because the normal load can be expanded as a double Fourier series in x_1 and x_2, it suffices to consider loads of the form

$$\sigma_{13} = \sigma_{23} = 0 \qquad \text{at} \qquad x_3 = \pm H/2$$

$$\sigma_{33}(x_1, x_2, \pm H/2) = p^{\pm} \sin r x_1 \sin s x_2 \tag{5}$$

where p^+ and p^- are known constants, $r = k\pi/L_1$, $s = m\pi/L_2$, and k and m are positive integers. The thermal boundary conditions on the top and the bottom surfaces are specified as

$$\vartheta^{\pm} T(x_1, x_2, \pm H/2) + \xi^{\pm} q_3(x_1, x_2, \pm H/2)$$

$$= \varphi^{\pm} \sin r x_1 \sin s x_2 \tag{6}$$

When values of constants $\vartheta^{\pm}$ and $\xi^{\pm}$ are chosen appropriately, various boundary conditions corresponding to either a prescribed temperature, a prescribed heat flux, or an exposure to an ambient temperature through a boundary conductance can be specified.

The interfaces between adjoining layers are assumed to be perfectly bonded together and in ideal thermal contact so that

$$[\![u_i]\!] = 0 \tag{7a}$$

$$[\![\sigma_{i3}]\!] = 0 \tag{7b}$$

$$[\![T]\!] = 0 \tag{7c}$$

$$[\![q_3]\!] = 0 \tag{7d}$$

on $x_3 = H^{(2)}, H^{(3)}, \ldots, H^{(N)}$. Here $[\![u_i]\!]$ is the jump in the value of u_i across an interface.

The mechanical and the thermal problems are one-way coupled in the sense that the temperature field is determined first by solving Eqs. (1b) and (2b) and the pertinent boundary conditions, and the displacements are later obtained from Eqs. (1a) and (2a) and the relevant boundary conditions.

III.   Exact Solution

We construct a local rectangular Cartesian coordinate system $x_1^{(n)}, x_2^{(n)}$, and $x_3^{(n)}$ with local axes parallel to the global axes and the origin at the point where the global x_3 axis intersects the mid-surface of the nth lamina. In the local coordinate system, the nth lamina occupies the region $[0, L_1] \times [0, L_2] \times [-h^{(n)}/2, h^{(n)}/2]$, where $h^{(n)} = H^{(n+1)} - H^{(n)}$. We drop the superscript n for convenience with the understanding that all material constants and variables belong to this layer.

We assume that, within each layer, the Lamé constants λ and μ, the stress-temperature modulus β, and the thermal conductivity κ

are analytic functions of x_3 and, thus, can be represented by a Taylor series expansion about its midsurface as

$$[\lambda, \mu, \beta, \kappa] = \sum_{\alpha=0}^{\infty} \left[\tilde{\lambda}^{(\alpha)}, \tilde{\mu}^{(\alpha)}, \tilde{\beta}^{(\alpha)}, \tilde{\kappa}^{(\alpha)}\right] x_3^{\alpha} \tag{8}$$

Note that λ, μ, β, and κ are positive quantities for all x_3, and therefore, $\tilde{\lambda}^{(0)}$, $\tilde{\mu}^{(0)}$, $\tilde{\beta}^{(0)}$, and $\tilde{\kappa}^{(0)}$ are positive.

A. Temperature Field

A solution for the change in temperature of points in the nth layer is sought in the form

$$T = \theta(x_3) \sin r x_1 \sin s x_2 \tag{9}$$

The assumed temperature function T identically satisfies the boundary conditions (4c) and (4f) at the edges of the plate. Substitution for T from Eq. (9) into Eq. (2b) and the result into Eq. (1b) gives the following second-order ordinary differential equation with variable coefficients:

$$\kappa[(r^2 + s^2)\theta - \theta''] - \kappa'\theta' = 0 \tag{10}$$

where a prime denotes derivative with respect to x_3. We assume a solution for θ in the form of a power series

$$\theta(x_3) = \sum_{\gamma=0}^{\infty} \tilde{\theta}^{(\gamma)} x_3^{\gamma} \tag{11}$$

The series (11) and the Taylor series for κ in Eq. (8) are substituted into Eq. (10). By multiplying the infinite series, appropriately shifting the index of summation, and equating each power of x_3 to zero, we obtain the following recurrence relation:

$$\sum_{\gamma=0}^{\alpha} \tilde{\kappa}^{(\gamma)} \left[\tilde{\theta}^{(\alpha-\gamma+2)}(\alpha-\gamma+2)(\alpha-\gamma+1) - \tilde{\theta}^{(\alpha-\gamma)}(r^2+s^2)\right]$$

$$+ \tilde{\kappa}^{(\gamma+1)}\tilde{\theta}^{(\alpha-\gamma+1)}(\gamma+1)(\alpha-\gamma+1) = 0 \tag{12}$$

for $\alpha = 0, 1, 2, \ldots$. Because $\tilde{\kappa}^{(0)} \neq 0$, corresponding to $\alpha = 0$ in Eq. (12), we obtain

$$\tilde{\theta}^{(2)} = [(r^2 + s^2)/2]\tilde{\theta}^{(0)} - \left[\tilde{\kappa}^{(1)} \big/ 2\tilde{\kappa}^{(0)}\right]\tilde{\theta}^{(1)} \tag{13}$$

Evaluation of the recursion formula (12) successively for $\alpha = 1, 2, \ldots$, gives $\tilde{\theta}^{(\alpha+2)}$ in terms of arbitrary constants $\tilde{\theta}^{(0)}$ and $\tilde{\theta}^{(1)}$. Substitution for $\tilde{\theta}^{(\alpha)}$ into Eq. (11) and and the result into Eq. (9) gives the following expression for the temperature change:

$$T = \left[\tilde{\theta}^{(0)}\psi^{(0)}(x_3) + \tilde{\theta}^{(1)}\psi^{(1)}(x_3)\right] \sin r x_1 \sin s x_2 \tag{14}$$

where $\psi^{(0)}(x_3)$ and $\psi^{(1)}(x_3)$ are known infinite series and $\tilde{\theta}^{(0)}$ and $\tilde{\theta}^{(1)}$ are unknown constants. There are two unknown constants for each layer, which result in a total of $2N$ unknowns for an N-layer plate. The constants are determined by satisfying the thermal boundary conditions (6) on the top and the bottom surfaces of the plate and the interface continuity conditions (7c) and (7d) for the thermal quantities between adjoining layers. This gives two conditions for the top and the bottom surfaces and two conditions at each of the $N - 1$ interfaces. The resulting system of $2N$ linear algebraic equations for the $2N$ unknowns is readily solved to yield the change in temperature and the heat flux vector for the entire plate.

B. Displacement Field

A solution for the displacement field in the nth layer is sought in the form

$$u_1 = U_1(x_3) \cos r x_1 \sin s x_2, \qquad u_2 = U_2(x_3) \sin r x_1 \cos s x_2$$

$$u_3 = U_3(x_3) \sin r x_1 \sin s x_2 \tag{15}$$

which identically satisfies the homogeneous boundary conditions (4a–4b) and (4d–4e) at the simply supported edges. Substitution for

u from Eq. (15) into Eq. (3), for ε and also for T from Eq. (9) into Eq. (2a), and then for σ into Eq. (1a) gives the following coupled system of second-order ordinary differential equations:

$$(\lambda + 2\mu)U_1 r^2 + \lambda U_2 rs + \mu\left(U_1 s^2 + U_2 rs\right) - \lambda U_3' r$$

$$- \mu'(U_1' + U_3 r) - \mu(U_1'' + U_3' r) + \beta\theta r = 0$$

$$(\lambda + 2\mu)U_2 s^2 + \lambda U_1 rs + \mu\left(U_2 s^2 + U_1 rs\right) - \lambda U_3' s$$

$$- \mu'(U_2' + U_3 s) - \mu(U_2'' + U_3' s) + \beta\theta s = 0$$

$$\mu(U_1' r + U_2' s) + \mu U_3(r^2 + s^2) + \lambda'(U_1 r + U_2 s) + \lambda(U_1' r + U_2' s)$$

$$- (\lambda' + 2\mu')U_3' - (\lambda + 2\mu)U_3'' + \beta'\theta + \beta\theta' = 0 \tag{16}$$

We assume a power series solution for the displacements as

$$U_i(x_3) = \sum_{\gamma=0}^{\infty} \tilde{U}_i^{(\gamma)} x_3^{\gamma} \tag{17}$$

Inserting into the differential equations (16) the Taylor series for the material properties λ, μ, and β from Eq. (8) and the assumed power series solution for the displacements and the temperature change from Eqs. (17) and (11), we obtain the following recurrence relations for every nonnegative integer α:

$$\sum_{\gamma=0}^{\alpha} \left(\tilde{\lambda}^{(\gamma)} + 2\tilde{\mu}^{(\gamma)}\right)\tilde{U}_1^{(\alpha-\gamma)}r^2 + \tilde{\lambda}^{(\gamma)}\tilde{U}_2^{(\alpha-\gamma)}rs$$

$$+ \tilde{\mu}^{(\gamma)}\left(\tilde{U}_1^{(\alpha-\gamma)}s^2 + \tilde{U}_2^{(\alpha-\gamma)}rs\right) - (\alpha-\gamma+1)\tilde{\lambda}^{(\gamma)}\tilde{U}_3^{(\alpha-\gamma+1)}r$$

$$- (\gamma+1)\tilde{\mu}^{(\gamma+1)}\left((\alpha-\gamma+1)\tilde{U}_1^{(\alpha-\gamma+1)} + \tilde{U}_3^{(\alpha-\gamma)}r\right)$$

$$- (\alpha-\gamma+1)\tilde{\mu}^{(\gamma)}\left((\alpha-\gamma+2)\tilde{U}_1^{(\alpha-\gamma+2)} + \tilde{U}_3^{(\alpha-\gamma+1)}r\right)$$

$$+ \tilde{\beta}^{(\gamma)}\tilde{\theta}^{(\alpha-\gamma)}r = 0$$

$$\sum_{\gamma=0}^{\alpha} \left(\tilde{\lambda}^{(\gamma)} + 2\tilde{\mu}^{(\gamma)}\right)\tilde{U}_2^{(\alpha-\gamma)}s^2 + \tilde{\lambda}^{(\gamma)}\tilde{U}_1^{(\alpha-\gamma)}rs$$

$$+ \tilde{\mu}^{(\gamma)}\left(\tilde{U}_2^{(\alpha-\gamma)}r^2 + \tilde{U}_1^{(\alpha-\gamma)}rs\right) - (\alpha-\gamma+1)\tilde{\lambda}^{(\gamma)}\tilde{U}_3^{(\alpha-\gamma+1)}s$$

$$- (\gamma+1)\tilde{\mu}^{(\gamma+1)}\left((\alpha-\gamma+1)\tilde{U}_2^{(\alpha-\gamma+1)} + \tilde{U}_3^{(\alpha-\gamma)}s\right)$$

$$- (\alpha-\gamma+1)\tilde{\mu}^{(\gamma)}\left((\alpha-\gamma+2)\tilde{U}_2^{(\alpha-\gamma+2)} + \tilde{U}_3^{(\alpha-\gamma+1)}s\right)$$

$$+ \tilde{\beta}^{(\gamma)}\tilde{\theta}^{(\alpha-\gamma)}s = 0$$

$$\sum_{\gamma=0}^{\alpha} \tilde{\mu}^{(\gamma)}(\alpha-\gamma+1)\left(\tilde{U}_1^{(\alpha-\gamma+1)}r + \tilde{U}_2^{(\alpha-\gamma+1)}s\right)$$

$$+ \tilde{\mu}^{(\gamma)}\tilde{U}_3^{(\alpha-\gamma)}(r^2+s^2) + (\gamma+1)\tilde{\lambda}^{(\gamma+1)}\left(\tilde{U}_1^{(\alpha-\gamma)}r + \tilde{U}_2^{(\alpha-\gamma)}s\right)$$

$$+ (\alpha-\gamma+1)\tilde{\lambda}^{(\gamma)}\left(\tilde{U}_1^{(\alpha-\gamma+1)}r + \tilde{U}_2^{(\alpha-\gamma+1)}s\right)$$

$$- (\gamma+1)(\alpha-\gamma+1)\left(\tilde{\lambda}^{(\gamma+1)} + 2\tilde{\mu}^{(\gamma+1)}\right)\tilde{U}_3^{(\alpha-\gamma+1)}$$

$$- (\alpha-\gamma+2)(\alpha-\gamma+1)\left(\tilde{\lambda}^{(\gamma)} + 2\tilde{\mu}^{(\gamma)}\right)\tilde{U}_3^{(\alpha-\gamma+2)}$$

$$- \tilde{\beta}^{(\gamma+1)}\tilde{\theta}^{(\alpha-\gamma)}(\gamma+1) - \tilde{\beta}^{(\gamma)}\tilde{\theta}^{(\alpha-\gamma+1)}(\alpha-\gamma+1) = 0 \tag{18}$$

The recurrence relations (18) are evaluated successively for $\alpha = 0, 1, \ldots$, to obtain $\tilde{U}_1^{(\alpha+2)}$, $\tilde{U}_2^{(\alpha+2)}$, and $\tilde{U}_3^{(\alpha+2)}$ in terms of arbitrary constants $\tilde{U}_1^{(0)}$, $\tilde{U}_1^{(1)}$, $\tilde{U}_2^{(0)}$, $\tilde{U}_2^{(1)}$, $\tilde{U}_3^{(0)}$, and $\tilde{U}_3^{(1)}$. Thus, there are six unknown constants for each layer, resulting in a total of $6N$ unknowns for an N-layer plate. The constants are determined by satisfying the mechanical boundary conditions (5) on the top and the bottom surfaces of the plate and the interface continuity conditions

(7a) and (7b) for the mechanical quantities between adjoining layers. This yields six conditions for the top and the bottom surfaces and six conditions at each of the $N - 1$ interfaces. The resulting system of $6N$ linear algebraic equations for the $6N$ unknowns is solved to obtain displacements and stresses for the entire plate.

The semi-inverse method of analyzing simply supported plate problems as assumed in Eqs. (9) and (15) is due to Vlasov,[30] Srinivas and Rao,[31−33] and Pagano[34] and has been adopted by others to study piezoelectric and thermoelastic plate problems. Vel and Batra[35−37] have used the Eshelby−Stroh formalism to analyze deformations of plates with arbitrary boundary conditions prescribed at the edges.

IV. Plate Theories

The displacement field for the CPT,[24,25] the FSDT,[26,27] and the TSDT[13,27,28] can be written as

$$u_\gamma(x_i) = u_\gamma^0 - x_3 u_{3,\gamma}^0 + g(x_3)\varphi_\gamma \qquad (19a)$$

$$u_3(x_i) = u_3^0 \qquad (19b)$$

where u_γ^0, u_3^0, and φ_γ are independent of x_3 and the function $g(x_3) = 0$ for the CPT, $g(x_3) = x_3$ for the FSDT, and $g(x_3) = x_3(1 - 4x_3^2/3h^2)$ for the TSDT. In this section, the Latin indices range from 1 to 3 and the Greek indices from 1 to 2. Functions $\boldsymbol{u}^0$ give displacements of a point on the midsurface of the plate and $(\varphi_1 - u_{3,1}^0)$ and $(-\varphi_2 + u_{3,2}^0)$ are, respectively, the rotations of the transverse normal to the midsurface about the x_2 and x_1 axes. Displacement fields (19) were proposed for studying isothermal deformations of a plate; here we use them to analyze thermomechanical deformations in the presence of temperature gradients in the thickness direction. Cheng and Batra,[10] among others, employed these displacement fields for analyzing thermomechanical deformations of a functionally graded plate.

For the bending of a linear functionally graded plate subjected to an arbitrary distributed normal load $p(x_\gamma)$ on its surface, the field equations are

$$N_{\gamma\eta,\eta} = 0, \qquad M_{\gamma\eta,\gamma\eta} + p = 0, \qquad P_{\gamma\eta,\eta} - \mathcal{K}R_\gamma = 0 \quad (20)$$

where

$$[N_{\gamma\eta}, M_{\gamma\eta}, P_{\gamma\eta}] = \int_{-H/2}^{H/2} \sigma_{\gamma\eta}[1, x_3, g]\,\mathrm{d}x_3$$

$$R_\gamma = \int_{-H/2}^{H/2} \sigma_{\gamma3}g_{,3}\,\mathrm{d}x_3$$

$$\sigma_{\gamma\eta} = H_{\gamma\eta\omega\rho}\varepsilon_{\omega\rho} - \beta\delta_{\gamma\eta}T, \qquad \sigma_{\gamma3} = 2E_{\gamma3\omega3}\varepsilon_{\omega3} \quad (21)$$

and constant $\mathcal{K}$ is the shear correction factor used only for the FSDT. We set $\mathcal{K} = \frac{5}{6}$, although this value was proposed by Reissner for a homogeneous plate. Because the temperature T is assumed to be known in the CPT, the FSDT, and the TSDT, we substitute the exact value for the temperature field from Eq. (9) into Eq. (21). The transverse normal stress σ_{33} is assumed to be negligible and neglected in all three plate theories; this is inconsistent with the assumption of zero transverse normal strain implied by Eq. (19b). For an isotropic material,

$$H_{\gamma\eta\omega\rho} = [\nu E/(1 - \nu^2)]\delta_{\gamma\eta}\delta_{\omega\rho} + [E/2(1 + \nu)](\delta_{\gamma\omega}\delta_{\eta\rho} + \delta_{\gamma\rho}\delta_{\eta\omega})$$

$$E_{\gamma3\omega3} = \mu\delta_{\gamma\omega} \qquad (22)$$

where E, ν, and μ are, respectively, Young's modulus, Poisson's ratio, and the shear modulus. For a functionally graded plate, material properties are assumed to vary in the thickness direction only, that is, $E = E(x_3)$, $\nu = \nu(x_3)$, and $\mu = \mu(x_3)$.

The boundary conditions for a simply supported plate are

$$N_{11} = 0, \qquad M_{11} = 0, \qquad P_{11} = 0, \qquad u_3^0 = 0$$

$$u_2^0 = 0, \qquad \varphi_2 - u_{3,2}^0 = 0 \qquad \text{at} \qquad x_1 = 0, L_1$$

$$N_{22} = 0, \qquad M_{22} = 0, \qquad P_{22} = 0, \qquad u_3^0 = 0$$

$$u_1^0 = 0, \qquad \varphi_1 - u_{3,1}^0 = 0 \qquad \text{at} \qquad x_2 = 0, L_2 \quad (23)$$

A solution to the partial differential equations (20) can be obtained by choosing the displacements and rotations as

$$[u_1^0, \varphi_1] = [S_1, S_2]\cos rx_1 \sin sx_2$$

$$[u_2^0, \varphi_2] = [S_3, S_4]\sin rx_1 \cos sx_2$$

$$u_3^0 = S_5 \sin rx_1 \sin sx_2 \qquad (24)$$

The assumed fields (24) satisfy boundary conditions (23) identically. Substitution from Eq. (24) into Eq. (21) and the result into Eq. (20) yields five simultaneous linear equations for the five unknowns S_k, which can be readily solved. The transverse shear stresses σ_{13} and σ_{23} and the transverse normal stress σ_{33} are obtained by integrating the three-dimensional equilibrium equations in the thickness direction.

V. Effective Moduli of Two-Phase Composites

Consider a functionally graded composite material that is fabricated by mixing two distinct material phases, for example, a metal and a ceramic. Often, precise information about the size, shape, and distribution of the particles may not be available, and the effective moduli of the graded composite must be evaluated based only on the volume fraction distributions and the approximate shape of the dispersed phase. Several micromechanics models have been developed over the years to infer the effective properties of macroscopically homogeneous composite materials. We summarize two popular methods for estimating the effective properties, the Mori–Tanaka and the self-consistent methods, and use them to analyze functionally graded materials.

A. Mori–Tanaka Estimate

The Mori–Tanaka (see Refs. 15, 17, and 23) scheme for estimating the effective moduli is applicable to regions of the graded microstructure that have a well-defined continuous matrix and a discontinuous particulate phase as shown in Fig. 1a. It takes into
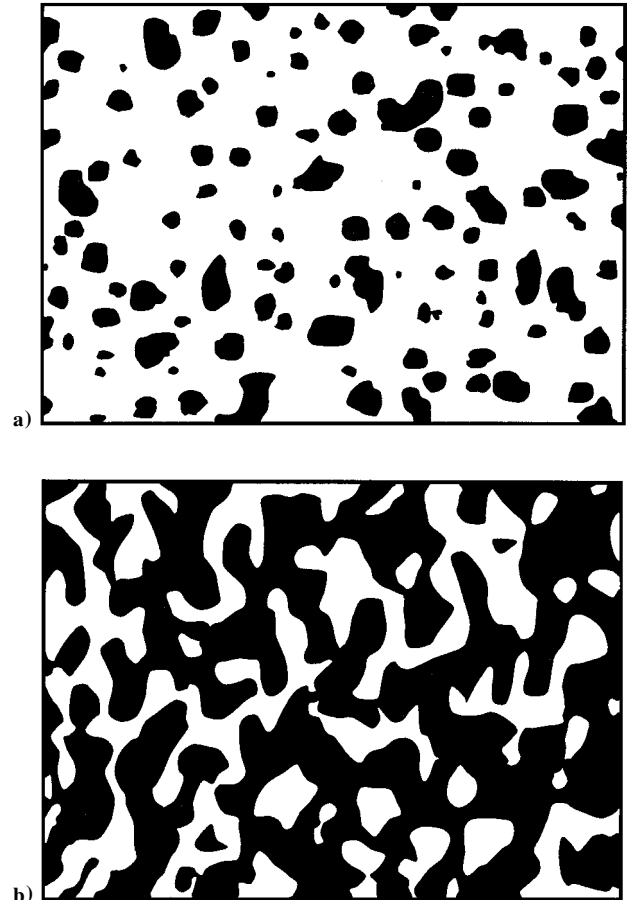

Fig. 1 Two-phase material with a) particulate microstructure and b) skeletal microstructure.

account the interaction of the elastic fields between neighboring inclusions. It is assumed that the matrix phase, denoted by the subscript 1, is reinforced by spherical particles of a particulate phase, denoted by the subscript 2. In this notation, K_1, μ_1, κ_1, and α_1 are the bulk modulus, the shear modulus, the thermal conductivity, and the thermal expansion coefficient, respectively, and V_1 is the volume fraction of the matrix phase. K_2, μ_2, κ_2, α_2, and V_2 are the corresponding material properties and the volume fraction of the particulate phase. Note that $V_1 + V_2 = 1$, that the Lamé constant λ is related to the bulk and the shear moduli by $\lambda = K - 2\mu/3$, and that the stress-temperature modulus is related to the modulus of thermal expansion by $\beta = (3\lambda + 2\mu)\alpha = 3K\alpha$. The following estimates for the effective local bulk modulus K and shear modulus μ are useful for a random distribution of isotropic particles in an isotropic matrix:

$$\frac{K - K_1}{K_2 - K_1} = V_2 \left/ \left[1 + (1 - V_2)\frac{K_2 - K_1}{K_1 + \left(\frac{4}{3}\right)\mu_1} \right] \right.$$

$$\frac{\mu - \mu_1}{\mu_2 - \mu_1} = V_2 \left/ \left[1 + (1 - V_2)\frac{\mu_2 - \mu_1}{\mu_1 + f_1} \right] \right. \tag{25}$$

where $f_1 = \mu_1(9K_1 + 8\mu_1)/6(K_1 + 2\mu_1)$. The effective thermal conductivity κ is given by[38]

$$\frac{\kappa - \kappa_1}{\kappa_2 - \kappa_1} = \frac{V_2}{1 + (1 - V_2)(\kappa_2 - \kappa_1)/3\kappa_1} \tag{26}$$

and the coefficient of thermal expansion α is determined from the correspondence relation[39]

$$\frac{\alpha - \alpha_1}{\alpha_2 - \alpha_1} = \frac{1/K - 1/K_1}{1/K_2 - 1/K_1} \tag{27}$$

B. Self-Consistent Estimate

The self-consistent method[15,18] assumes that each reinforcement inclusion is embedded in a continuum material whose effective properties are those of the composite. This method does not distinguish between matrix and reinforcement phases, and the same overall moduli is predicted in another composite in which the roles of the phases are interchanged. This makes it particularly suitable for determining the effective moduli in those regions that have an interconnected skeletal microstructure as shown in Fig. 1b. The locally effective moduli by the self-consistent method are

$$\delta/K = V_1/(K - K_2) + V_2/(K - K_1) \tag{28a}$$

$$\eta/\mu = V_1/(\mu - \mu_2) + V_2/(\mu - \mu_1) \tag{28b}$$

where $\delta = 3 - 5\eta = K/(K + 4\mu/3)$. These are implicit expressions for the unknowns K and μ. Equation (28a) can be solved for K in terms of μ to obtain

$$K = 1/[V_1/(K_1 + 4\mu/3) + V_2/(K_2 + 4\mu/3)] - 4\mu/3 \tag{29}$$

and μ is obtained by solving the following quartic equation:

$$\frac{V_1 K_1}{K_1 + 4\mu/3} + \frac{V_2 K_2}{K_2 + 4\mu/3} + 5\left(\frac{V_1\mu_2}{\mu - \mu_2} + \frac{V_2\mu_1}{\mu - \mu_1}\right) + 2 = 0 \tag{30}$$

The self-consistent estimate of the thermal conductivity coefficient[40] is in the implicit form

$$\frac{V_1(\kappa_1 - \kappa)}{\kappa_1 + 2\kappa} + \frac{V_2(\kappa_2 - \kappa)}{\kappa_2 + 2\kappa} = 0 \tag{31}$$

The self-consistent estimate of α is obtained by substitution of the self-consistent estimate of the bulk modulus K from Eq. (29) into the correspondence relation (27). Because the quartic equation (30) and the quadratic equation (31) have to be solved to obtain the shear modulus μ and the thermal conductivity κ, it is easier to use the Mori–Tanaka method than the self-consistent scheme.

VI. Results and Discussion

Here we present exact results for a representative simply supported square plate with its top surface subjected to either a mechanical load or a thermal load:

$$[\sigma_{33}(x_1, x_2, H/2), T(x_1, x_2, H/2)]$$

$$= [p^+, T^+] \sin(\pi x_1/L_1) \sin(\pi x_2/L_2) \tag{32}$$

The bottom surface is traction free and held at the reference temperature, that is, $\sigma_{i3}(x_1, x_2, -H/2) = 0$ and $T(x_1, x_2, -H/2) = 0$.

Because it is common in high-temperature applications to employ a ceramic top layer as a thermal barrier to a metallic structure, we choose the constituent materials of the functionally graded plate to be Al and SiC with the following material properties.[11] For Al, $E_m = 70$ GPa, $v_m = 0.3$, $\alpha_m = 23.4 \times 10^{-6}$/K, and $\kappa_m = 233$ W/mK. For SiC, $E_c = 427$ GPa, $v_c = 0.17$, $\alpha_c = 4.3 \times 10^{-6}$/K, $\kappa_c = 65$ W/mK. Recall that the bulk modulus and the shear modulus are related to Young's modulus E and Poisson's ratio v by $K = E/3(1 - 2v)$ and $\mu = E/2(1 + v)$. We assume that the volume fraction of the ceramic phase is given by the power-law-type function

$$V_c = V_c^- + \left(V_c^+ - V_c^-\right)\left(\tfrac{1}{2} + x_3/H\right)^n \tag{33}$$

Here V_c^+ and V_c^- are the volume fractions of the ceramic phase on the top and the bottom surfaces of the plate, respectively, and n is a parameter that dictates the volume fraction profile through the thickness. Cheng and Batra[10] have also used a similar power law function for the volume fraction, except that they have assumed $V_c^+ = 1$ and $V_c^- = 0$. We performed a convergence study for the temperature and displacements. All results reported here have less than 0.001% truncation error and are computed by retaining 200 terms in the series expansion for the temperature and displacements in Eqs. (11) and (17), respectively.

The physical quantities are nondimensionalized by relations

$$[\bar{u}_1, \bar{u}_2] = \frac{100 E_m H^2[u_1, u_2]}{p^+ L_1^3}, \qquad \bar{u}_3 = \frac{100 E_m H^3 u_3}{p^+ L_1^4}$$

$$[\bar{\sigma}_{11}, \bar{\sigma}_{22}, \bar{\sigma}_{12}] = \frac{10 H^2[\sigma_{11}, \sigma_{22}, \sigma_{12}]}{p^+ L_1^2}$$

$$[\bar{\sigma}_{13}, \bar{\sigma}_{23}] = \frac{10 H[\sigma_{13}, \sigma_{23}]}{p^+ L_1}, \qquad \bar{\sigma}_{33} = \frac{\sigma_{33}}{p^+} \tag{34}$$

for the applied mechanical load and by

$$\hat{T} = \frac{T}{T^+}, \qquad \hat{q}_3 = -\frac{q_3 H}{\kappa_m T^+}, \qquad [\hat{u}_1, \hat{u}_2] = \frac{10[u_1, u_2]}{\alpha_m T^+ L_1}$$

$$\hat{u}_3 = \frac{100 H u_3}{\alpha_m T^+ L_1^2}, \qquad [\hat{\sigma}_{11}, \hat{\sigma}_{22}, \hat{\sigma}_{12}] = \frac{10[\sigma_{11}, \sigma_{22}, \sigma_{12}]}{E_m \alpha_m T^+}$$

$$[\hat{\sigma}_{13}, \hat{\sigma}_{23}] = \frac{100 L_1[\sigma_{13}, \sigma_{23}]}{E_m \alpha_m T^+ H}, \qquad \hat{\sigma}_{33} = \frac{100 L_1^2 \sigma_{33}}{E_m \alpha_m T^+ H^2} \tag{35}$$

for the thermal load. Nondimensional quantities for the mechanical load are denoted by a superimposed bar and those for the thermal load by a superimposed caret.

Consider a simply supported metal–ceramic square plate ($L_2 = L_1$) with the metal (Al) taken as the matrix phase and the ceramic (SiC) taken as the particulate phase. That is, $P_1 = P_m$ and $P_2 = P_c$, where P is either the volume fraction V or any material property. The exact solution for displacements and stresses at specific points in the plate is compared with the CPT, the FSDT, and the TSDT results in Fig. 2 for length-to-thickness ratio L_1/H ranging from 2 to 40. The effective material properties are obtained by the Mori–Tanaka scheme. The transverse deflection $\bar{u}_3(L_1/2, L_2/2, 0)$ of the plate centroid for the mechanical load predicted by the FSDT and the TSDT is in excellent agreement with the exact solution even for thick plates with $L_1/H < 10$, but the CPT solution exhibits significant error for thick plates. The error in the CPT value for the
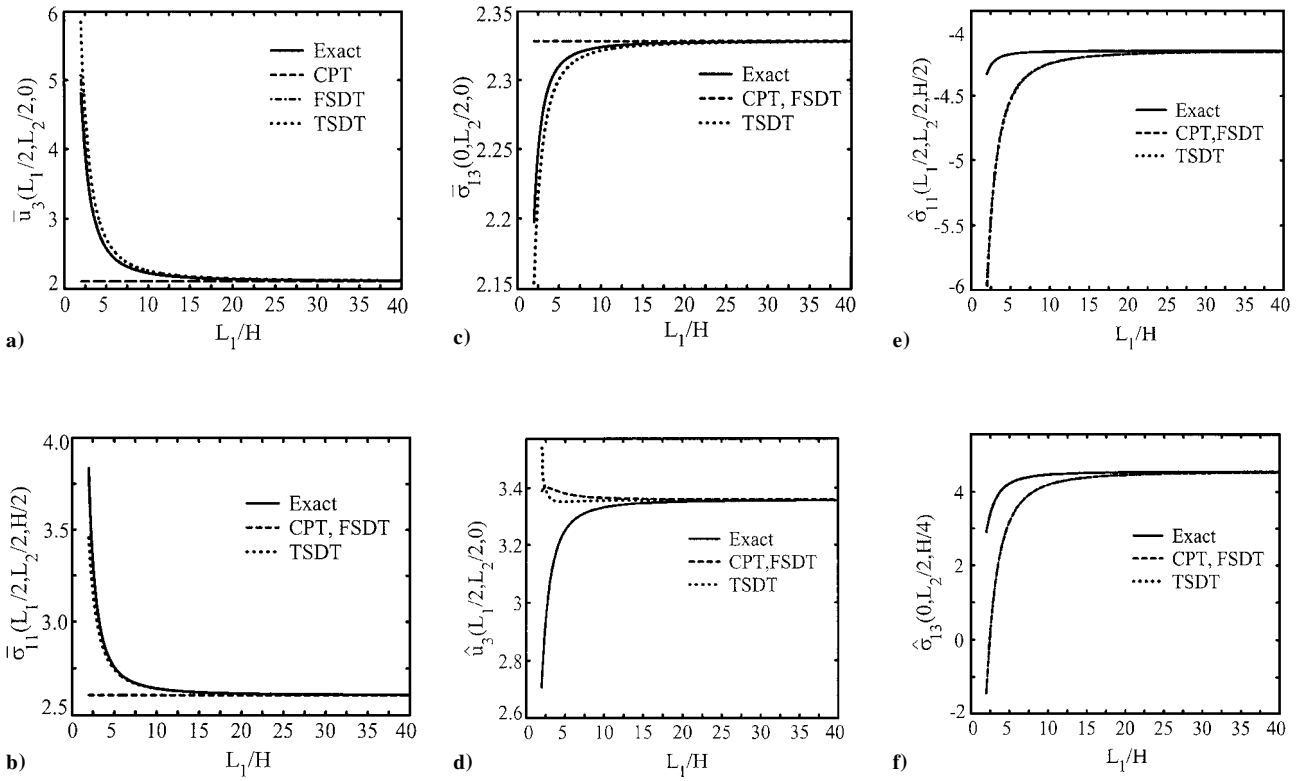
Fig. 2   Transverse deflection, longitudinal stress, and transverse shear stress vs length-to-thickness ratio for Al/SiC functionally graded square plate computed with Mori–Tanaka homogenization scheme, $V_c^- = 0$, $V_c^+ = 0.5$, and $n = 2$: a–c) mechanical load and d–f) thermal load.
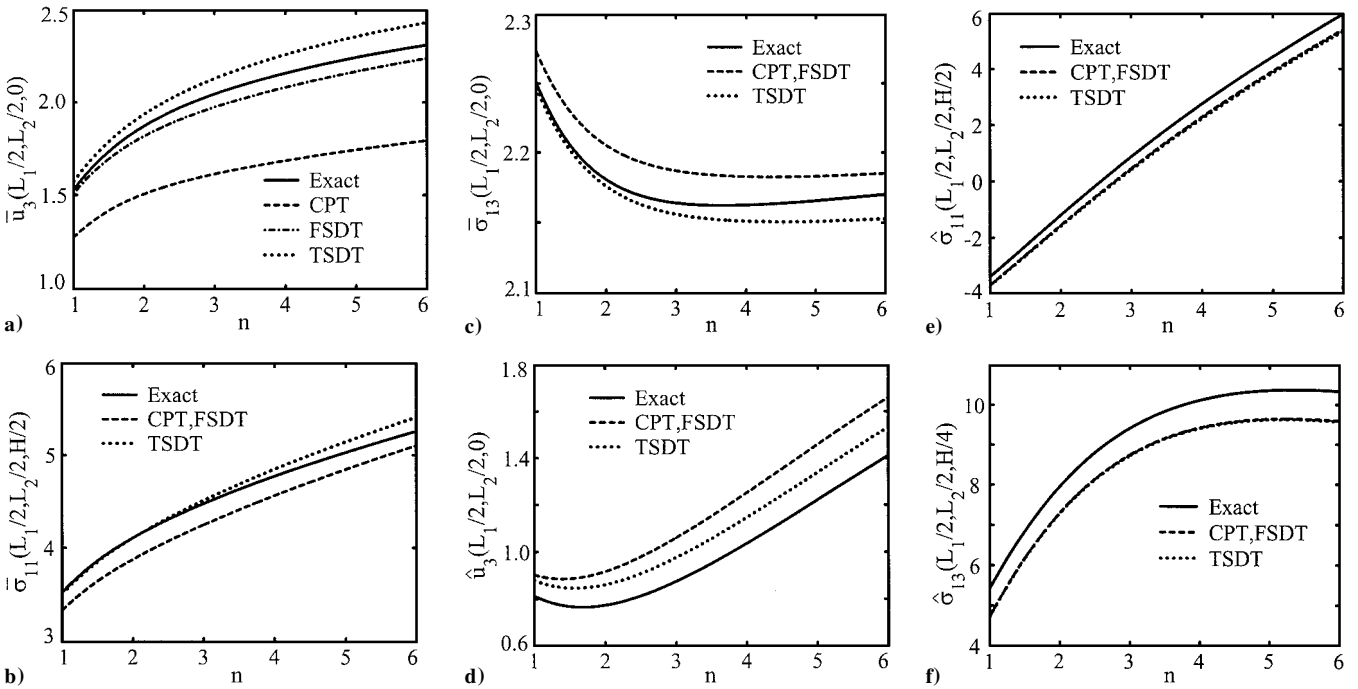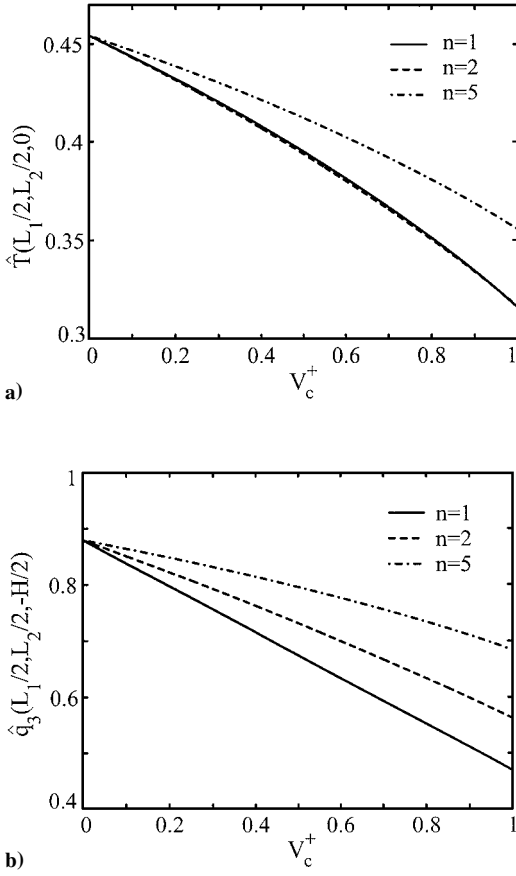

Fig. 3   Transverse deflection, longitudinal stress, and transverse shear stress vs power law index n for Al/SiC functionally graded square plate computed with Mori–Tanaka homogenization scheme, $V_c^- = 0$, $V_c^+ = 1.0$, and $L_1/H = 5$: a–c) mechanical load and d–f) thermal load.

transverse deflection can be attributed to the large shear deformation that occurs in thick plates. The CPT and the FSDT give identical values of the longitudinal stress $\bar{\sigma}_{11}$ and of the transverse shear stress $\bar{\sigma}_{13}$, which deviate from the exact solution as the length-to-thickness ratio decreases. The TSDT gives accurate results for $\bar{\sigma}_{11}$ and $\bar{\sigma}_{13}$ even for thick plates. When the plate is subjected to the thermal load, both the longitudinal stress $\hat{\sigma}_{11}$ and the transverse shear stress $\hat{\sigma}_{13}$ given by each one of the three plate theories are inaccurate for thick plates with $L_1/H < 10$. This could be due to the neglect

of transverse normal strains and the transverse normal stresses in the plate theories. Furthermore, the displacement fields in the plate theories are constructed assuming isothermal conditions and need to be modified when thermal gradients are present, as is the case in the present problem. Note that the transverse shear and normal stresses have been computed by integrating the three-dimensional elasticity equations in the thickness direction.

Figure 3 shows plots of the nondimensional values of the transverse displacement u_3 of the plate centroid, the longitudinal stress

Fig. 4 **Temperature at the center and heat flux on the bottom surface of Al/SiC functionally graded square plate vs volume fraction of ceramic on the top surface for power law index $n = 1$, 2, and 5 computed with Mori–Tanaka homogenization scheme, $V_c^- = 0$, and $L_1/H = 5$.**

σ_{11}, and the transverse shear stress σ_{13} vs the power law index n for a thick square plate ($L_1/H = 5$). The effective properties are obtained by the Mori–Tanaka scheme, and the volume fraction V_c of the ceramic phase is taken to be 0 and 1 on the bottom and the top surfaces, respectively. It is seen that the differences between the exact values and the CPT, the FSDT, and the TSDT values of these quantities for the thermal load do not change appreciably for increasing values of the power law index n. However, for the mechanical load, applied on the top surface of the plate, the errors in the transverse deflection of the plate centroid and the stresses computed with each one of the three plate theories increase with an increase in the value of n. Whereas the CPT and the FSDT underpredict, the TSDT overpredicts the transverse displacement at the plate centroid and the longitudinal stress at the centroid of the top surface. For the thermal load, all three plate theories underpredict this longitudinal stress. For the mechanical load, the transverse shear stress at the plate centroid computed from the TSDT solution is lower than that obtained from the exact solution, but the CPT and the FSDT give a value higher than that obtained from the analytical solution. For the thermal load, all three plate theories yield essentially the same value of the transverse shear stress at the point ($L_1/2$, $L_2/2$, $H/4$) and this value is lower than the analytical one.

The change in temperature $\hat{T}(L_1/2, L_2/2, 0)$ at the plate centroid vs the ceramic volume fraction V_c^+ on the top surface for the thermal load is shown in Fig. 4a. It is clear that the temperature change decreases monotonically with an increase in the value of V_c^+. The nondimensional transverse component of the heat flux on the bottom surface, shown in Fig. 4b, decreases as the ceramic volume fraction on the top surface increases because the thermal conductivity of the ceramic phase is much smaller than that of the metallic phase. Figure 5 shows plots of the transverse displacements of the plate centroid and components of the stress at specific points in the plate vs the ceramic volume fraction on the top surface. As is evident from Figs. 5a–5f, the percentage errors in the transverse displacement of the plate centroid and stresses at the chosen points obtained from the plate theories do not change appreciably with the value of the ceramic volume fraction on the top surface. For both the
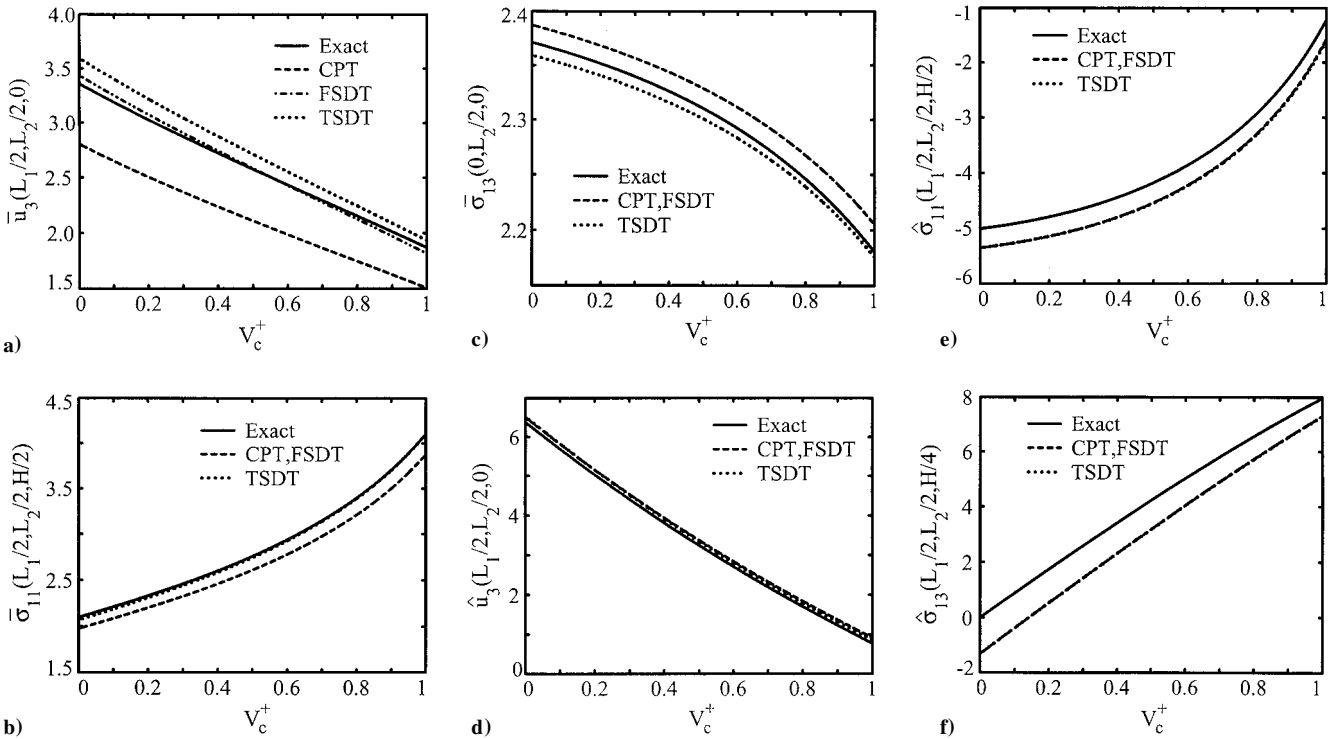
Fig. 5 **Transverse deflection, longitudinal stress, and transverse shear stress vs ceramic volume fraction on the top surface of Al/SiC functionally graded square plate computed with Mori–Tanaka homogenization scheme, $V_c^- = 0$, $n = 2$, and $L_1/H = 5$: a-c) mechanical load and d-f) thermal load.**

Table 1   Exact displacements, stresses, temperature, and heat flux at specific locations for the Al/SiC functionally graded square plate when subjected to mechanical and temperature loads: Mori–Tanaka scheme

Variable	$V_c^- = 0, V_c^+ = 0.5, n = 2$			$V_c^- = 0, n = 2, L_1/H = 5$		
	$L_1/H = 5$	$L_1/H = 10$	$L_1/H = 40$	$V_c^+ = 0.2$	$V_c^+ = 0.6$	$V_c^+ = 1$
$\bar{u}_1(0, L_2/2, H/2)$	−2.9129	−2.8997	−2.8984	−3.6982	−2.6708	−1.7421
$\bar{u}_3(L_1/2, L_2/2, 0)$	2.5748	2.2266	2.1163	3.0254	2.4326	1.8699
$\bar{u}_3(L_1/2, L_2/2, H/2)$	2.5559	2.2148	2.1155	2.9852	2.4196	1.8767
$\bar{\sigma}_{11}(L_1/2, L_2/2, H/2)$	2.7562	2.6424	2.6093	2.3285	2.9359	4.1042
$\bar{\sigma}_{12}(0, 0, H/2)$	−1.5600	−1.5529	−1.5522	−1.2163	−1.7106	−2.8534
$\bar{\sigma}_{13}(0, L_2/2, 0)$	2.3100	2.3239	2.3281	2.3516	2.2918	2.1805
$\bar{\sigma}_{33}(L_1/2, L_2/2, H/4)$	0.8100	0.8123	0.8129	0.8300	0.8024	0.7623
$\hat{T}(L_1/2, L_2/2, 0)$	0.3938	0.4240	0.4343	0.4315	0.3800	0.3162
$\hat{q}_3(L_1/2, L_2/2, -H/2)$	0.7316	0.8075	0.8335	0.8219	0.7001	0.5625
$\hat{u}_1(0, L_2/2, H/2)$	−1.2101	−1.2124	−1.2131	−1.6989	−1.0624	−0.5326
$\hat{u}_3(L_1/2, L_2/2, 0)$	3.2497	3.3312	3.3567	5.0302	2.7110	0.7741
$\hat{u}_3(L_1/2, L_2/2, H/2)$	4.4111	3.6337	3.3758	6.5843	3.7561	1.4115
$\hat{\sigma}_{11}(L_1/2, L_2/2, H/2)$	−4.1764	−4.1555	−4.1492	−4.7912	−3.8561	−1.2077
$\hat{\sigma}_{12}(0, 0, H/2)$	−6.4804	−6.4928	−6.4966	−5.5878	−6.8047	−8.7240
$\hat{\sigma}_{13}(0, L_2/2, H/4)$	4.2264	4.4703	4.5501	1.7390	5.0227	7.9552
$\hat{\sigma}_{33}(L_1/2, L_2/2, 0)$	−8.6829	−9.1622	−9.3191	−3.5531	−10.3675	−17.3524
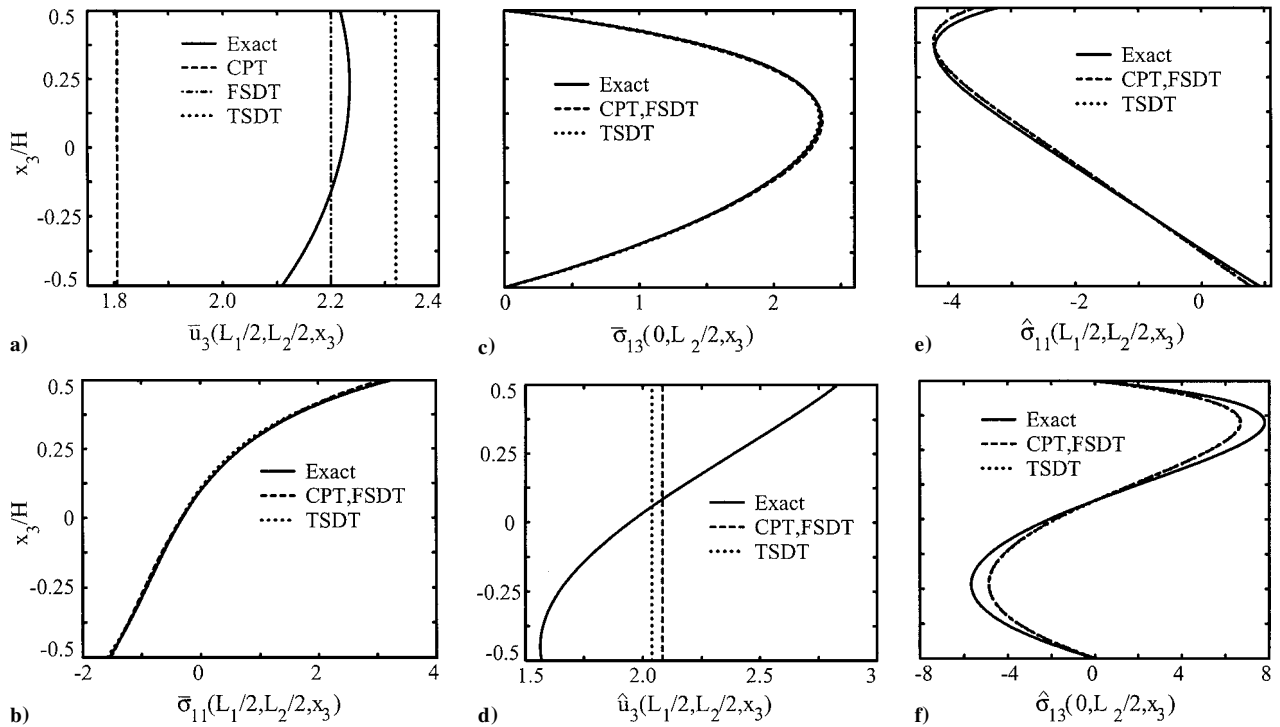

Fig. 6   Through-the-thickness variation of the transverse deflection and stresses in Al/SiC functionally graded square plate computed with Mori–Tanaka homogenization scheme, $V_c^- = 0$, $V_c^+ = 0.75$, $L_1/H = 5$, and $n = 2$: a–c) mechanical load and d–f) thermal load.

mechanical and the thermal loads, the transverse deflection of the plate centroid decreases nearly affinely with an increase in the value of V_c^+. However, the longitudinal stress at the centroid of the top surface increases parabolically with a rise in the value of V_c^+. With an increase in the value of V_c^+, the transverse shear stress decreases parabolically for the mechanical load, and it increases essentially linearly for the thermal load. Note that the transverse shear stresses are evaluated at different points for the two loads. The through-the-thickness variations of the displacements and longitudinal stresses at points on the centroidal axis and the shear stress variation at an edge are shown in Fig. 6 for a thick plate ($L_1/H = 5$). When subjected to the mechanical load, the TSDT overestimates the transverse deflection $\bar{u}_3$ at all points within the plate, the CPT underestimates it at all points, and the FSDT value of $\bar{u}_3$ is close to the average value given by the exact solution. It is clear that the thickness of the plate changes and that the transverse normal strain is not uniform through the plate thickness. The longitudinal stress $\bar{\sigma}_{11}$ does not vary as a linear function of the thickness coordinate x_3 because the

plate is functionally graded and the material properties are functions of x_3. The transverse shear stress $\bar{\sigma}_{13}$ attains its maximum value at $x_3 = 0.11H$. Note that all three plate theories give very good values of the longitudinal stress and the transverse shear stress. When the functionally graded thick plate with $L_1/H = 5$ is subjected to the temperature load, the error exhibited by both the CPT and the FSDT values for the transverse deflection $\hat{u}_3$ on the top surface is 26%. The corresponding error in the TSDT value for $\hat{u}_3$ is 28%. The large errors are due to the assumption of inextensibility of the normals to the midsurface inherent in all three plate theories considered here. The extensibility of transverse normals has been incorporated in plate theories proposed by Vidoli and Batra,[41] Batra and Vidoli,[42] Soldatos and Watson,[43] Kant,[44] Lee and Yu,[20] Lee et al.,[21] and others. Simmonds[45] showed that accurate three-dimensional stresses can be derived from the CPT by including the transverse extensibility effects. The transverse centroidal displacements and the stresses at the centroid of the top surface using the self-consistent scheme vs the length-to-thickness ratio are plotted in Fig. 7 for

Table 2 Exact displacements, stresses, temperature, and heat flux at specific locations for the Al/SiC functionally graded square plate when subjected to mechanical and temperature loads: self-consistent scheme

Variable	$V_c^- = 0.2, V_c^+ = 0.8, n = 2$			$V_c^- = 0.2, n = 2, L_1/H = 5$		
	$L_1/H = 5$	$L_1/H = 10$	$L_1/H = 40$	$V_c^+ = 0.3$	$V_c^+ = 0.5$	$V_c^+ = 0.7$
$\bar{u}_1(0, L_2/2, H/2)$	−1.7038	−1.6694	−1.6583	−2.8810	−2.3463	−1.8908
$\bar{u}_3(L_1/2, L_2/2, 0)$	1.6159	1.3960	1.3249	2.2957	1.9956	1.7297
$\bar{u}_3(L_1/2, L_2/2, H/2)$	1.6164	1.3921	1.3246	2.2693	1.9829	1.7268
$\bar{\sigma}_{11}(L_1/2, L_2/2, H/2)$	3.0504	2.9190	2.8775	2.1981	2.5302	2.8861
$\bar{\sigma}_{12}(0, 0, H/2)$	−2.0000	−1.9596	−1.9466	−1.1916	−1.4876	−1.8313
$\bar{\sigma}_{13}(0, L_2/2, 0)$	2.2624	2.2788	2.2815	2.3591	2.3254	2.2837
$\bar{\sigma}_{33}(L_1/2, L_2/2, H/4)$	0.7908	0.7941	0.7937	0.8344	0.8174	0.7994
$\hat{T}(L_1/2, L_2/2, 0)$	0.3636	0.3921	0.4018	0.4412	0.4123	0.3804
$\hat{q}_3(L_1/2, L_2/2, -H/2)$	0.5414	0.5984	0.6180	0.6898	0.6324	0.5721
$\hat{u}_1(0, L_2/2, H/2)$	−0.6325	−0.6338	−0.6339	−1.3954	−1.0477	−0.7531
$\hat{u}_3(L_1/2, L_2/2, 0)$	1.4036	1.4399	1.4492	4.1920	2.9097	1.8323
$\hat{u}_3(L_1/2, L_2/2, H/2)$	2.0583	1.6110	1.4601	5.4598	3.8984	2.5860
$\hat{\sigma}_{11}(L_1/2, L_2/2, H/2)$	−3.7621	−3.7399	−3.7372	−5.2147	−4.7038	−4.0586
$\hat{\sigma}_{12}(0, 0, H/2)$	−7.4246	−7.4397	−7.4415	−5.7715	−6.6431	−7.2940
$\hat{\sigma}_{13}(0, L_2/2, H/4)$	6.7961	7.1847	7.2838	1.2419	3.8282	6.0253
$\hat{\sigma}_{33}(L_1/2, L_2/2, 0)$	−13.8128	−14.5591	−14.9234	−2.5369	−7.8219	−12.2810
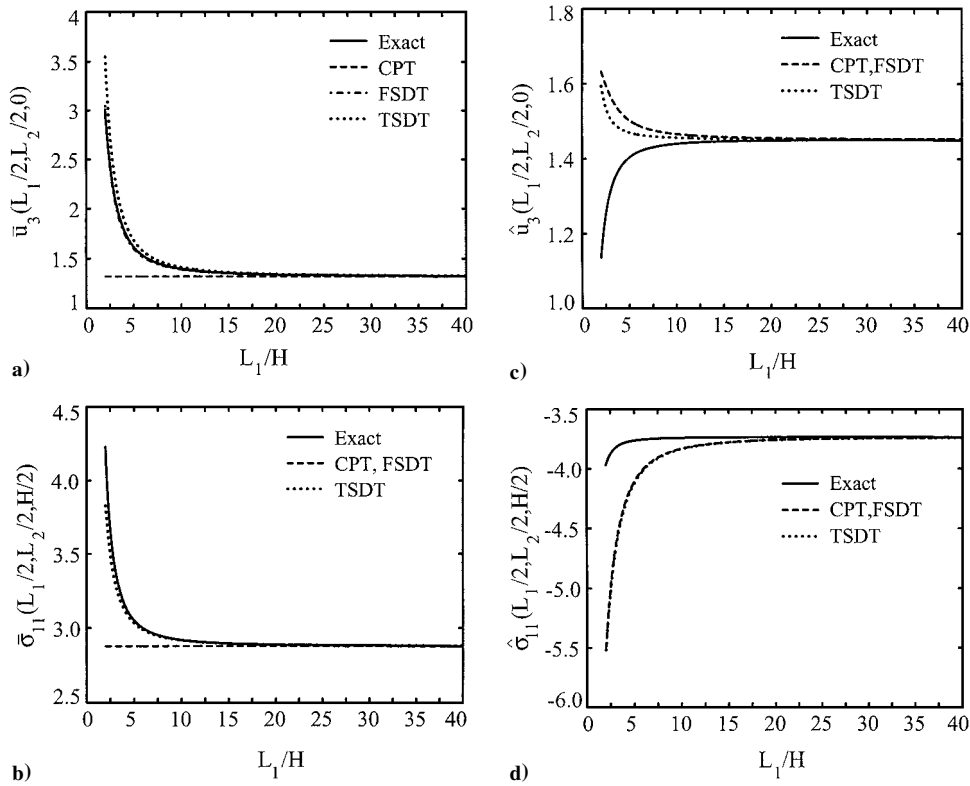
Fig. 7 Transverse deflection and longitudinal stress vs length-to-thickness ratio for Al/SiC functionally graded square plate obtained with self-consistent homogenization scheme, $V_c^- = 0.2$, $V_c^+ = 0.8$, and $n = 2$: a–c) mechanical load and d–f) thermal load.

$V_c^- = 0.2$, $V_c^+ = 0.8$, and $n = 2$. The plots are qualitatively similar to those obtained by using the Mori–Tanaka scheme and shown in Fig. 2.

We have listed in Tables 1 and 2 values of displacements, stresses, temperature, and heat flux at specific points in a simply supported Al/SiC functionally graded plate for the two loads considered. Values listed in Table 1 are obtained by using the Mori–Tanaka homogenization scheme and those in Table 2 by the self-consistent method. These should facilitate comparisons between the exact values and those obtained from plate theories or other approximate methods such as the finite element method. To capture well the through-the-thickness variation of material properties, a very fine mesh in the thickness direction and, hence, throughout the domain will be required. Results presented herein should help decide the degree of fineness of the mesh and/or the choice of elements.

In the examples studied so far, we used a single homogenization scheme (either the Mori–Tanaka method or the self-consistent method) to estimate the effective properties for the entire plate. This approach is appropriate only for functionally graded plates that have the same microstructure everywhere. Reiter and Dvorak[16] performed detailed finite element studies of the response of simulated discrete models containing both skeletal and particulate microstructures and concluded that homogenized models of combined microstructures that employ only a single averaging method do not provide reliable agreements with the discrete model predictions. However, close agreement with the discrete model was shown by homogenized models that employ different effective property estimates for regions of the plate that have different microstructures. They state that, in those parts of the graded microstructure that have a well-defined continuous matrix
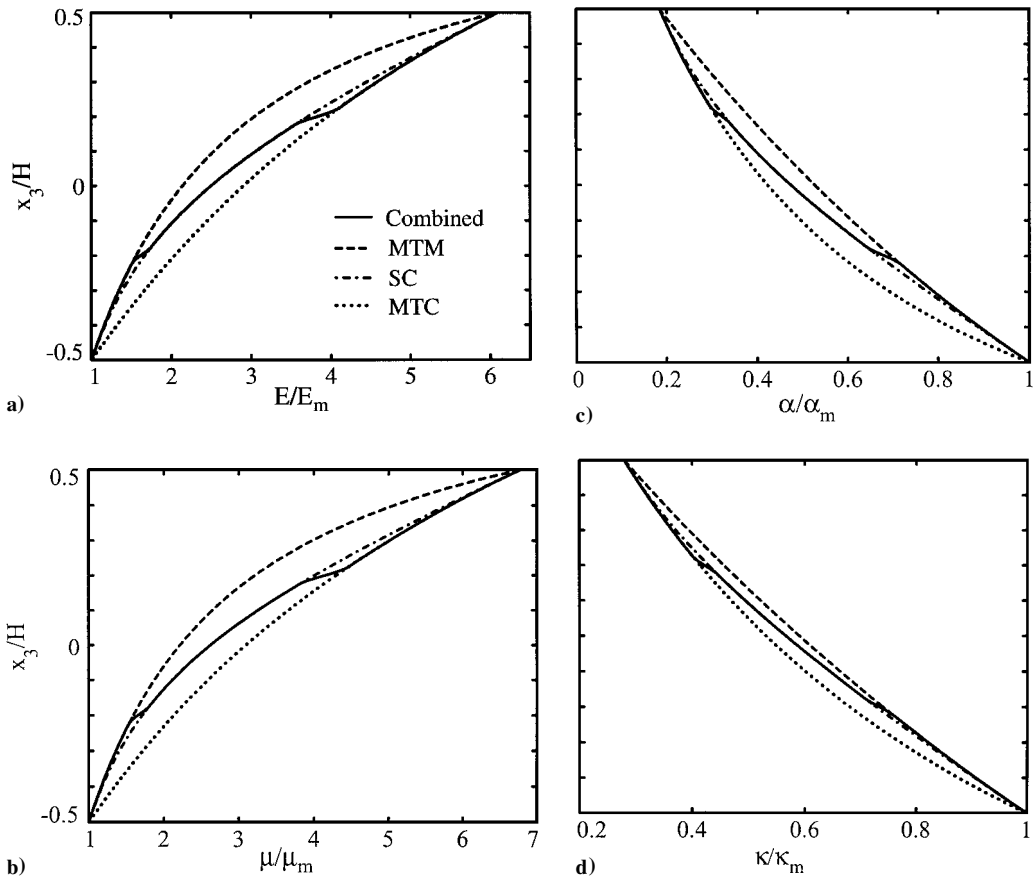
Fig. 8 Effective properties for a) Young's modulus, b) shear modulus, c) coefficient of thermal expansion, and d) thermal conductivity as a function of the thickness coordinate x_3 obtained by various homogenization schemes.
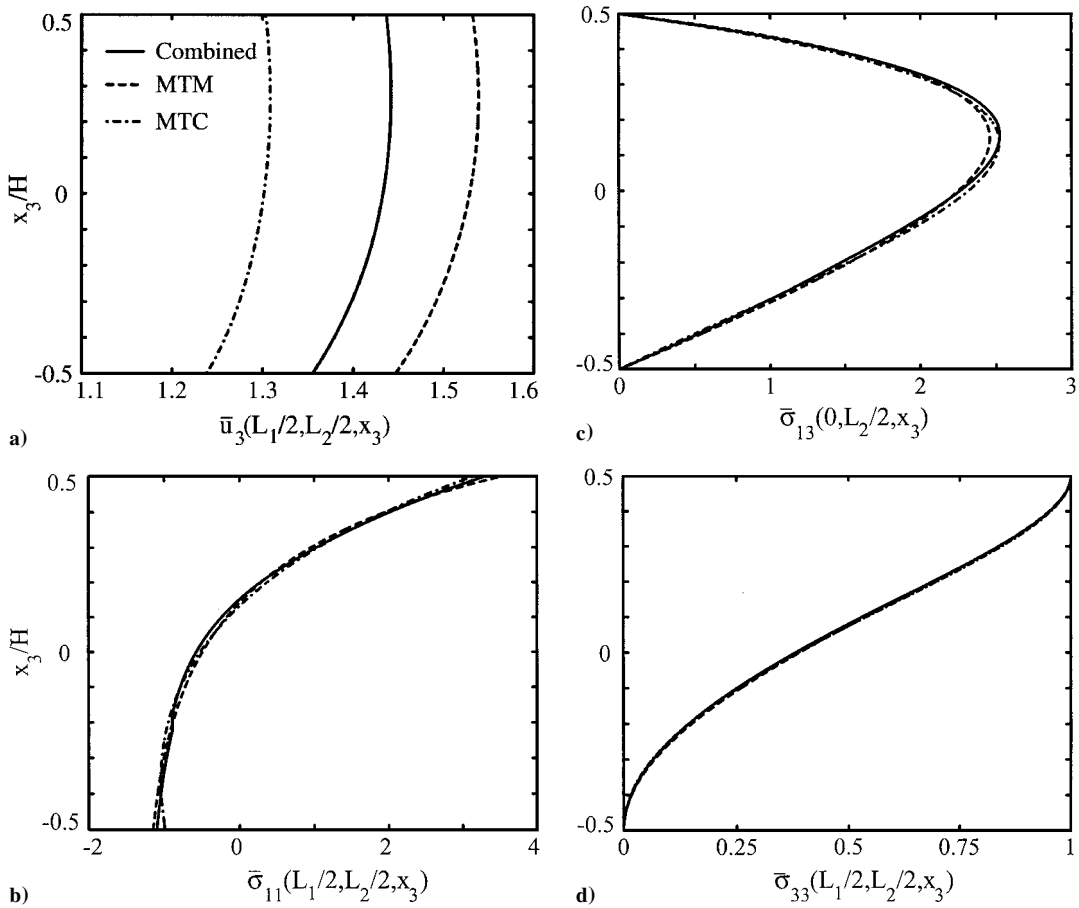

Fig. 9 Through-the-thickness variation of the transverse deflection and stresses in Al/SiC functionally graded square plate obtained by various homogenization schemes; mechanical load, $L_1/H = 5$.

and discontinuous reinforcement, the effective properties should be approximated by the appropriate Mori–Tanaka estimates and that, in skeletal microstructure that often form transition zones between clearly defined matrix and particulate phases, the effective properties should be approximated by the self-consistent method.

We consider a functionally graded plate that has an affine variation of the ceramic volume fraction given by $V_c = \frac{1}{2} + x_3/H$. It is assumed to have a well-defined continuous metallic matrix with discontinuous ceramic particles in the metal rich region $-0.5H \leq x_3 \leq -0.2H$ adjacent to the bottom surface and a well-defined continuous ceramic matrix with discontinuous metallic particles in the ceramic rich region $0.2H \leq x_3 \leq 0.5H$ adjacent to the top surface. The plate is assumed to have a skeletal microstructure in the central region $-0.2H \leq x_3 \leq 0.2H$. We use a combined model, wherein the effective properties in the metal rich region adjacent to the bottom surface are obtained by the Mori–Tanaka scheme with a metallic matrix phase (MTM), the effective properties in the ceramic rich region adjacent to the top surface are obtained by the Mori–Tanaka scheme with a ceramic matrix phase (MTC), and the effective material properties in the central region are obtained by the self-consistent scheme (SC). To accommodate the discontinuities in homogenized material properties predicted at the boundaries between the different regions, we employ the third-order transition functions used by Reiter and Dvorak[16] in transition regions of width $0.05H$ centered at $x_3 = -0.2H$ and $0.2H$. The through-the-thickness variations of the effective Young's modulus, shear modulus, coefficient of thermal expansion, and thermal conductivity obtained by the combined homogenization technique are plotted in Fig. 8. In Fig. 8, MTM, MTC, and SC signify effective properties obtained by using a single averaging method through the entire thickness of the plate.

In the combined model, there are five distinct regions in the thickness direction, namely, the three primary regions in which the effective properties are obtained by MTM, MTC, and SC and the two transition regions at the boundaries between them. Within each region, the effective material properties are expanded as a Taylor series, and the solution to the thermal and the mechanical equilibrium equations are obtained in terms of 8 unknown constants, resulting in a total of 40 unknowns. The constants are determined by satisfying the mechanical and the thermal boundary conditions (5) and (6) on the top and the bottom surfaces of the plate and the interface continuity conditions (7) for the thermal and the mechanical quantities between adjoining layers. This results in eight conditions for the top and the bottom surfaces and eight conditions at each of the four interfaces between regions with distinct micromechanical models. The resulting system of 40 linear algebraic equations for the 40 unknowns are solved to obtain the displacements and stresses for the entire plate.

A comparison of the through-the-thickness variation of the deflection and stresses obtained by the combined model and the two single averaging methods, namely, MTM and MTC, are shown in Fig. 9 for a thick plate ($L_1/H = 5$) subjected to the mechanical load. It is clear from Fig. 9a that there are significant differences in the values of the transverse deflection $\bar{u}_3$ given by the three homogenization techniques. However, the longitudinal stress $\bar{\sigma}_{11}$, the transverse shear stress $\bar{\sigma}_{13}$, and the transverse normal stress $\bar{\sigma}_{33}$ predicted by the three different homogenization methods are essentially the same. The corresponding displacements and stresses for the thermal load are shown in Fig. 10. The combined model gives a smaller value for the transverse deflection $\hat{u}_3$ than either the MTM or the MTC method. The magnitude of the longitudinal stress $\hat{\sigma}_{11}$ from the MTM method reaches a maximum value at a point situated slightly below the top surface. However, the maximum value of $\hat{\sigma}_{11}$ is predicted to occur on the top surface by the MTC and the combined model. Unlike the results for the mechanical load, the MTM, the MTC, and the combined model all give significantly different values for the transverse shear stress $\hat{\sigma}_{13}$ and the transverse normal stress $\hat{\sigma}_{33}$ for the thermal load.
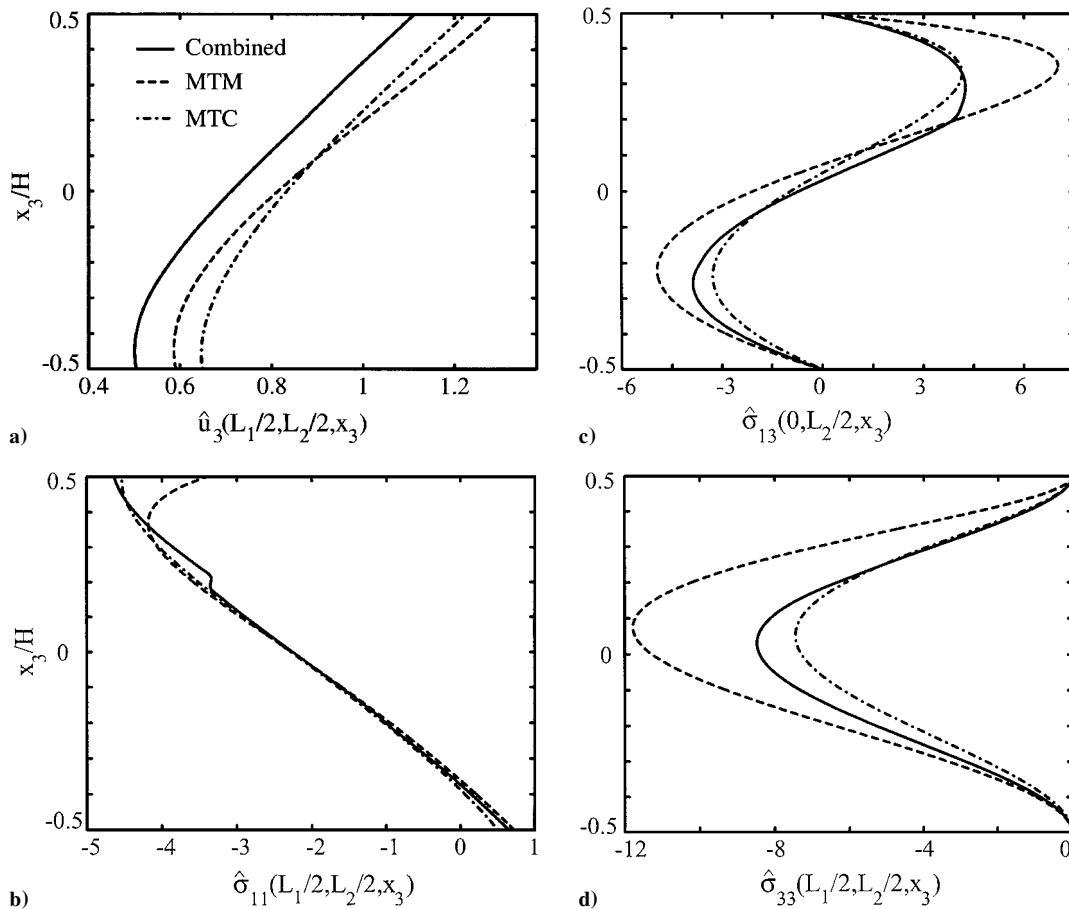

Fig. 10 Through-the-thickness variation of the transverse deflection and stresses in Al/SiC functionally graded square plate obtained by various homogenization schemes; thermal load, $L_1/H = 5$.

VII.   Conclusions

We have analyzed thermomechanical deformations of a simply supported functionally graded Al/SiC plate subjected to either a sinusoidal pressure or a sinusoidal temperature field on the top surface. The effective properties at points in the plate are obtained either by the Mori–Tanaka method, or the self-consistent scheme, or a combination of the two. The volume fractions of the constituents and, hence, the effective material properties are assumed to vary in the thickness direction only. The effective material properties, the three components of the displacement, and the temperature field are expanded in Taylor series in the thickness coordinate. When in-plane sinusoidal variations of the displacements and the temperature that identically satisfy boundary conditions at the edges are presumed, ordinary differential equations for functions giving their through-the-thickness variation are derived and solved analytically.

The exact solutions of the problems studied here are compared with those obtained by the classical plate theory, the FSDT, and the TSDT. For thick functionally graded plates, there are significant differences between the exact solution and that obtained with any one of these three plate theories even when the transverse normal and the transverse shear stresses are computed by integrating the three-dimensional elasticity equations. These differences could be due to displacement fields employed in plate theories that were originally proposed for studying isothermal deformations of a plate. It is found that the displacements, stresses, and temperatures computed with either the Mori–Tanaka scheme, or the self-consistent method, or their combination agree qualitatively but differ quantitatively. For the thermal load, the differences in the transverse displacements, the transverse shear stresses, and the transverse normal stresses are noticeable, but those in the longitudinal stress are negligible except near the top loaded surface. For the mechanical load, only the transverse displacements computed with the three methods exhibit significant variations. For each load, the nonzero transverse normal strains vary through the plate thickness.

The exact solutions presented here provide benchmark results, which can be used to assess the adequacy of different plate theories and also to compare results obtained by other approximate methods such as the finite element method.

References

[1]Berger, R., Kwon, P., and Dharan, C. K. H., "High Speed Centrifugal Casting of Metal Matrix Composites," *5th International Symposium on Transport Phenomena and Dynamics of Rotating Machinery*, Maui, HI, 1994.

[2]Fukui, Y., "Fundamental Investigation of Functionally Gradient Materials Manufacturing System Using Centrifugal Force," *JSME International Journal Series III*, Vol. 34, No. 1, 1991, pp. 144–148.

[3]Choy, K.-L., and Felix, E., "Functionally Graded Diamond-Like Carbon Coatings on Metallic Substrates," *Materials Science and Engineering A*, Vol. 278, No. 1, 2000, pp. 162–169.

[4]Khor, K. A., and Gu, Y. W., "Effects of Residual Stress on the Performance of Plasma Sprayed Functionally Graded ZrO2/NiCoCrAlY Coatings," *Materials Science and Engineering A*, Vol. 277, No. 1–2, 2000, pp. 64–76.

[5]Lambros, A., Narayanaswamy, A., Santare, M. H., and Anlas, G., "Manufacturing and Testing of a Functionally Graded Material," *Journal of Engineering Materials and Technology*, Vol. 121, No. 2, 1999, pp. 488–493.

[6]Breval, E., Aghajanian, K., and Luszcz, S. J., "Microstructure and Composition of Alumina/Aluminum Composites Made by the Directed Oxidation of Aluminum," *Journal of the American Ceramic Society*, Vol. 73, No. 9, 1990, pp. 2610–2614.

[7]Manor, E., Ni, H., Levi, C. G., and Mehrabian, R., "Microstructure Evaluation of SiC/Al2O3/Al Alloy Composite Produced by Melt Oxidation," *Journal of the American Ceramic Society*, Vol. 26, No. 7, 1993, pp. 1777–1787.

[8]Rogers, T. G., Watson, P., and Spencer, A. J. M., "Exact Three-Dimensional Elasticity Solutions for Bending of Moderately Thick Inhomogeneous and Laminated Strips Under Normal Pressure," *International Journal of Solids and Structures*, Vol. 32, No. 12, 1995, pp. 1659–1673.

[9]Tarn, J. Q., and Wang, Y. M., "Asymptotic Thermoelastic Analysis of Anisotropic Inhomogeneous and Laminated Plates," *Journal of Thermal Stresses*, Vol. 18, No. 1, 1995, pp. 35–58.

[10]Cheng, Z. Q., and Batra, R. C., "Three-Dimensional Thermoelastic Deformations of a Functionally Graded Elliptic Plate," *Composites: Part B*, Vol. 31, No. 2, 2000, pp. 97–106.

[11]Tanaka, K., Tanaka, Y., Enomoto, K., Poterasu, V. F., and Sugano, Y., "Design of Thermoelastic Materials Using Direct Sensitivity and Optimization Methods. Reduction of Thermal Stresses in Functionally Gradient Materials," *Computer Methods in Applied Mechanics and Engineering*, Vol. 106, No. 1–2, 1993, pp. 271–284.

[12]Tanaka, K., Tanaka, Y., Watanabe, H., Poterasu, V. F., and Sugano, Y., "An Improved Solution to Thermoelastic Material Design in Functionally Gradient Materials: Scheme to Reduce Thermal Stresses," *Computer Methods in Applied Mechanics and Engineering*, Vol. 109, No. 3–4, 1993, pp. 377–389.

[13]Reddy, J. N., "Analysis of Functionally Graded Plates," *International Journal for Numerical Methods in Engineering*, Vol. 47, No. 1–3, 2000, pp. 663–684.

[14]Reiter, T., Dvorak, G. J., and Tvergaard, V., "Micromechanical Models for Graded Composite Materials," *Journal of the Mechanics and Physics of Solids*, Vol. 45, No. 8, 1997, pp. 1281–1302.

[15]Reiter, T., and Dvorak, G. J., "Micromechanical Modelling of Functionally Graded Materials," *IUTAM Symposium on Transformation Problems in Composite and Active Materials*, edited by Y. Bahei-El-Din and G. J. Dvorak, Kluwer Academic, London, 1997, pp. 173–184.

[16]Reiter, T., and Dvorak, G. J., "Micromechanical Models for Graded Composite Materials: II. Thermomechanical Loading," *Journal of the Mechanics and Physics of Solids*, Vol. 46, No. 9, 1998, pp. 1655–1673.

[17]Mori, T., and Tanaka, K., "Average Stress in Matrix and Average Elastic Energy of Materials with Misfitting Inclusions," *Acta Metallurgica*, Vol. 21, 1973, pp. 571–574.

[18]Hill, R., "A Self-Consistent Mechanics of Composite Materials," *Journal of the Mechanics and Physics of Solids*, Vol. 13, No. 2, 1965, pp. 213–222.

[19]Cheng, Z. Q., and Batra, R. C., "Deflection Relationships Between the Homogeneous Kirchhoff Plate Theory and Different Functionally Graded Plate Theories," *Archives of Mechanics*, Vol. 52, No. 1, 2000, pp. 143–158.

[20]Lee, P. C. Y., and Yu, J.-D., "Governing Equations for a Piezoelectric Plate with Graded Properties Across the Thickness," *IEEE Tansactions on Ultrasonics, Ferroelectrics, and Frequency Control*, Vol. 45, No. 1, 1998, pp. 236–250.

[21]Lee, P. C. Y., Yu, J.-D., and Shih, W.-H., "Piezoelectric Ceramic Disks with Thickness Graded Material Properties," *IEEE Tansactions on Ultrasonics, Ferroelectrics, and Frequency Control*, Vol. 46, No. 1, 1999, pp. 205–215.

[22]Batra, R. C., "Finite Plane Strain Deformations of Rubberlike Materials," *International Journal for Numerical Methods in Engineering*, Vol. 15, No. 1, 1980, pp. 145–160.

[23]Benveniste, Y., "A New Approach to the Application of Mori–Tanaka's Theory of Composite Materials," *Mechanics of Materials*, Vol. 6, 1987, pp. 147–157.

[24]Jones, R. M., *Mechanics of Composite Materials*, Scripta, Washington, DC, 1975.

[25]Hyer, M. W., *Stress Analysis of Fiber-Reinforced Composite Materials*, McGraw-Hill Higher Education, New York, 1998.

[26]Whitney, J. M., and Pagano, N. J., "Shear Deformation in Heterogeneous Anisotropic Plates," *Journal of Applied Mechanics*, Vol. 37, No. 4, 1970, pp. 1031–1036.

[27]Reddy, J. N., *Mechanics of Laminated Composite Plates: Theory and Analysis*, CRC Press, Boca Raton, FL, 1997.

[28]Reddy, J. N., "A Simple Higher-Order Theory for Laminated Composite Plates," *Journal of Applied Mechanics*, Vol. 51, No. 4, 1984, pp. 745–752.

[29]Carlson, D. E., "Linear Thermoelasticity," *Handbuch der Physik, VIa/2*, Springer, Berlin, 1972.

[30]Vlasov, B. F., "On One Case of Bending of Rectangular Thick Plates," *Vestnik Moskovskogo Universiteta. Seriëïa Matematici Mekhaniki, Astronomii, Fiziki, Khimii*, Vol. 2, No. 2, 1957, pp. 25–34.

[31]Srinivas, S., and Rao, A. K., "A Note on Flexure of Thick Rectangular Plates and Laminates with Variation of Temperature Across Thickness," *Bulletin of the Polish Academy of Science, Technical Sciences*, Vol. 20, No. 2, 1972, pp. 229–234.

[32]Srinivas, S., and Rao, A. K., "Buckling of Thick Rectangular Plates," *AIAA Journal*, Vol. 7, No. 8, 1969, pp. 1645, 1646.

[33]Srinivas, S., and Rao, A. K., "Bending, Vibration and Buckling of Simply Supported Thick Orthotropic Rectangular Plates and Laminates," *International Journal of Solids and Structures*, Vol. 6, No. 10, 1970, pp. 1463–1481.

[34]Pagano, N. J., "Influence of Shear Coupling in Cylindrical Bending of Anisotropic Laminates," *Journal of Composite Materials*, Vol. 4, No. 3, 1970, pp. 330–343.

[35]Vel, S. S., and Batra, R. C., "Analytical Solution for Rectangular Thick Laminated Plates Subjected to Arbitrary Boundary Conditions," *AIAA Journal*, Vol. 37, No. 11, 1999, pp. 1464–1473.

[36]Vel, S. S., and Batra, R. C., "The Generalized Plane Strain Deformations of Anisotropic Composite Laminated Thick Plates," *International Journal of Solids and Structures*, Vol. 37, No. 5, 2000, pp. 715–733.

[37] Vel, S. S., and Batra, R. C., "Generalized Plane Strain Thermoelastic Deformation of Laminated Anisotropic Thick Plates," *International Journal of Solids and Structures*, Vol. 38, No. 8, 2001, pp. 1395–1414.

[38] Hatta, H., and Taya, M., "Effective Thermal Conductivity of a Misoriented Short Fiber Composite," *Journal of Applied Physics*, Vol. 58, No. 7, 1985, pp. 2478–2486.

[39] Rosen, B. W., and Hashin, Z., "Effective Thermal Expansion Coefficients and Specific Heats of Composite Materials," *International Journal of Engineering Science*, Vol. 8, 1970, pp. 157–173.

[40] Hashin, Z., "Assessment of the Self Consistent Scheme Approximation: Conductivity of Particulate Composites," *Journal of Composite Materials*, Vol. 2, 1968, pp. 284–300.

[41] Vidoli, S., and Batra, R. C., "Derivation of Plate and Rod Equations for a Piezoelectric Body from a Mixed Three-Dimensional Variational Principle," *Journal of Elasticity*, Vol. 59, Nos. 1/3, 2000, pp. 23–50.

[42] Batra, R. C., and Vidoli, S., "Higher-Order Piezoelectric Plate Theory Derived from a Three-Dimensional Variational Principle," *AIAA Journal*, Vol. 40, No. 1, 2002, pp. 91–104.

[43] Soldatos, K. P., and Watson, P., "Accurate Stress Analysis of Laminated Plates Combining Two-Dimensional Theory with the Exact Three-Dimensional Solution for Simply-Supported Edges," *Mathematics and Mechanics of Solids*, Vol. 2, No. 4, 1997, pp. 459–489.

[44] Kant, T., "Numerical Analysis of Thick Plates," *Computational Methods in Applied Mechanics and Engineering*, Vol. 31, No. 1, 1982, pp. 1–18.

[45] Simmonds, J. G., "An Improved Estimate for the Error in the Classical Linear Theory of Plate Bending," *Quarterly of Applied Mathematics*, Vol. 29, No. 3, 1971, pp. 439–447.

A. M. Waas
Associate Editor